

ENTROPY STABLE FINITE DIFFERENCE (ESFD) METHODS VIA ENTROPY CORRECTION ARTIFICIAL VISCOSITY (ECAV) AND KNAPSACK LIMITING (KL) TECHNIQUES*

BRIAN CHRISTNER[†] AND JESSE CHAN[‡]

Abstract. Entropy stable methods have become increasingly popular in the field of computational fluid dynamics. They often work by satisfying some form of a discrete entropy inequality: a discrete form of the 2nd law of thermodynamics. Schemes which satisfy a (semi-)discrete entropy inequality typically behave much more robustly, and do so in a way that is hyperparameter free. Recently, a new strategy was introduced to construct entropy stable discontinuous Galerkin methods: knapsack limiting, which blends together a low order, positivity preserving, and entropy stable scheme with a high order accurate scheme, in order to produce a high order accurate, entropy stable, and positivity preserving scheme. Another recent strategy introduces an entropy correction artificial viscosity into a high order scheme, aiming to satisfy a cell entropy inequality.

In this work, we introduce the techniques of knapsack limiting and artificial viscosity for finite difference discretizations. The proposed schemes preserve high order accuracy in sufficiently smooth conditions, are entropy stable, and are hyperparameter free. Moreover, the proposed knapsack limiting scheme provably preserves positivity for the compressible Euler and Navier-Stokes equations. Both schemes achieve this goal without significant performance tradeoffs compared to state of the art stabilized schemes.

Key words. Entropy Stable, Positivity Preserving, Finite Difference Methods

MSC codes. 68Q25, 68R10, 68U05

1. Introduction. In computational science, particularly when addressing multi-dimensional systems, numerically solving partial differential equations (PDEs) is critical. A classical method for numerically approximating the solutions to PDEs is the finite difference method. One of the primary advantages of finite difference methods are their ability to achieve arbitrarily high spatial accuracy by using wide stencils. Moreover, they are often the simplest and most computationally inexpensive schemes to implement. This makes them a valuable tool for capturing fine details of complex systems. The high order accuracy enables the numerical solution to approximate the true solution with a coarser mesh, reducing the computational time and resource expenditure.

Despite its advantages, high order finite difference methods are not without limitations, the most notable being a lack of robustness. High order methods often exhibit robustness issues or may fail to converge to accurate solutions. In response, essentially non-oscillatory (ENO) and weighted ENO (WENO) schemes have been proposed to mitigate these issues. These schemes can be applied to finite difference to construct an arbitrarily high order method, whose resulting simulations avoid oscillations around shocks. These schemes can also be used to construct solutions which satisfy nodal bounds. For instance, they can be used to satisfy positivity of density and pressure for the compressible Euler and Navier-Stokes equations. Though WENO schemes avoid oscillations in their simulations, they are generally not provably entropy stable [5].

One alternate approach to constructing high order numerical methods which

*

Funding: Supported by National Science Foundation awards DMS-1943186 and DMS-223148.

[†]Department of Computational Applied Mathematics and Operations Research, Rice University (bc71@rice.edu).

[‡]Oden Institute for Computational Engineering and Sciences and Department of Aerospace Engineering and Engineering Mechanics, The University of Texas at Austin (jesse.chan@oden.utexas.edu).

has gained traction within computational fluid dynamics (CFD) are discontinuous Galerkin (DG) methods. A common approach to resolve issues of robustness within DG methods is to satisfy a cell entropy inequality. The resulting methods are often called entropy stable DG (ESDG) methods. They often work by satisfying a (semi-)discrete entropy inequality: a discrete form of the 2nd law of thermodynamics. When discretizing conservation laws, it is often the case that the 2nd law of thermodynamics is not satisfied under discretization. By enforcing such an inequality, the resulting solutions typically behave much more robustly, and do so in a way that is hyperparameter free.

A recent technique for enforcing semi-discrete entropy stability for nodal DG methods, also known as DG spectral element methods (DGSEM), is *knapsack limiting*. At each right-hand-side evaluation, knapsack limiting optimally blends together a low order, entropy stable, positivity preserving update, with the high order accurate update coming from DGSEM. The resulting update is entropy stable, arbitrarily high order accurate in smooth regions, and satisfies a relative positivity condition. Moreover, it was shown in theory [20] and in practice [10, 4] that the resulting scheme preserves high order accuracy in sufficiently smooth regions. The methods developed in this paper are related to knapsack limiting, and utilize the same conceptual approach of computing optimal stabilization parameters using an optimization formulation with an inexpensive solver.

Another recent strategy in the field of DG methods for satisfying a semi-discrete entropy inequality are entropy correction artificial viscosity methods [1]. This scheme introduces an artificial viscosity into a high order accurate update, in order to satisfy a cell entropy inequality. The resulting methods are much more intuitive than the knapsack limiting scheme. This resulting scheme also exhibits arbitrarily high order accuracy for sufficiently regular cases.

In this work, we introduce the techniques of artificial viscosity entropy correction from the field of DG methods into the realm of finite difference methods. The first proposed scheme, entropy correction artificial viscosity for finite differences (ECAV-FD) preserves high order accuracy in sufficiently smooth regions, is entropy stable, and is parameter free. The second proposed scheme, knapsack limiting for finite differences (KL-FD) is a generalization of the ECAV-FD scheme, which can also provably preserve positivity.

2. High Order Finite Difference Methods. We will now discuss the finite difference discretization, for which we will utilize summation by parts (SBP) finite difference operators. For the sake of brevity, we will only describe how to construct SBP operators in $d \in \{1, 2\}$ dimensions, with the note that extension to higher dimensions is possible. The derived schemes will be written in such a way that an arbitrary number of dimensions are applicable.

We consider a hyperbolic conservation law imposed over domain $\Omega \subseteq \mathbb{R}^d$ with the imposed fluxes $\mathbf{f}_k : \mathbb{R}^v \rightarrow \mathbb{R}^v$:

$$(2.1) \quad \frac{\partial \mathbf{u}}{\partial t} + \sum_{k=1}^d \frac{\partial \mathbf{f}_k(\mathbf{u})}{\partial x_k} = \mathbf{0},$$

where $\mathbf{u} : \mathbb{R}^d \times [0, T] \rightarrow \mathbb{R}^v$, v is the number of variables, and T is the final time. The domain Ω is discretized using equally spaced points $\mathbf{x} \in \Omega$. n is the total number of nodes. The discretized solution can now be expressed $\mathbf{u} : [0, T] \rightarrow (\mathbb{R}^v)^n$, such that $\mathbf{u}(t)$ consists of pointwise evaluations of \mathbf{u} along the nodes \mathbf{x} . Now, we consider

$\mathbf{D}_1, \dots, \mathbf{D}_d \in \mathbb{R}^{n \times n}$ finite difference matrices of accuracy order N along each dimension. At this point, the conservation law can be discretized

$$(2.2) \quad \mathbf{M} \frac{d\mathbf{u}^H}{dt} + \sum_{k=1}^d (\mathbf{D}_k \mathbf{f}_k(\mathbf{u})) = \mathbf{0},$$

where $\mathbf{M} \in \mathbb{R}^{n \times n}$ is a diagonal mass matrix corresponding to $\mathbf{D}_1, \dots, \mathbf{D}_d$. An equivalent *flux-differencing* form can be derived:

$$(2.3) \quad \begin{aligned} \sum_{k=1}^d (\mathbf{D}_k \mathbf{f}_k(\mathbf{u}))_i &= \sum_{k=1}^d \sum_j 2\mathbf{D}_{k,ij} \left(\frac{\mathbf{f}_k(\mathbf{u}_i) + \mathbf{f}_k(\mathbf{u}_j)}{2} \right), \\ &= \sum_j \|\mathbf{n}_{ij}\| \cdot \left(\frac{\mathbf{f}(\mathbf{u}_i) + \mathbf{f}(\mathbf{u}_j)}{2} \cdot \frac{\mathbf{n}_{ij}}{\|\mathbf{n}_{ij}\|} \right), \end{aligned}$$

where $\mathbf{n}_{ij} \in \mathbb{R}^d$ is defined such that $\mathbf{n}_{ij,k} = 2\mathbf{D}_{k,ij}$, and $\mathbf{f} : \mathbb{R}^v \rightarrow \mathbb{R}^{v \times d}$, such that the k th column $(\mathbf{f}(\mathbf{u}))_k = \mathbf{f}_k(\mathbf{u})$. The relation on (2.3) arises from the property that $\mathbf{D}_k \mathbf{1} = \mathbf{0}$. Importantly,

$$(2.4) \quad \mathbf{f}^{\text{central}}(\mathbf{u}_i, \mathbf{u}_j, \hat{\mathbf{n}}_{ij}) = \left(\frac{\mathbf{f}(\mathbf{u}_i) + \mathbf{f}(\mathbf{u}_j)}{2} \cdot \hat{\mathbf{n}}_{ij} \right),$$

is known as the *central flux*. We can therefore generalize the discretization of the conservation law (2.1) as such:

$$(2.5) \quad \begin{aligned} \mathbf{M} \frac{d\mathbf{u}^H}{dt} + \mathbf{r}^H &= \mathbf{0}, \\ \mathbf{r}_i^H &= \sum_j \|\mathbf{n}_{ij}\| \mathbf{f}^{\text{vol}} \left(\mathbf{u}_i, \mathbf{u}_j, \frac{\mathbf{n}_{ij}}{\|\mathbf{n}_{ij}\|} \right), \end{aligned}$$

where \mathbf{r}^H is called the *high order volume term*, and \mathbf{f}^{vol} is a suitable volume flux, which satisfies the two following properties:

$$(2.6) \quad \begin{aligned} \mathbf{f}^{\text{vol}}(\mathbf{u}, \mathbf{u}, \hat{\mathbf{n}}) &= \mathbf{f}(\mathbf{u}) \cdot \hat{\mathbf{n}} && \text{Consistency,} \\ \mathbf{f}^{\text{vol}}(\mathbf{u}_i, \mathbf{u}_j, \hat{\mathbf{n}}_{ij}) &= -\mathbf{f}^{\text{vol}}(\mathbf{u}_j, \mathbf{u}_i, -\hat{\mathbf{n}}_{ij}) && \text{Skew-Symmetry.} \end{aligned}$$

We call this procedure *flux differencing* [6, 3]. The properties of \mathbf{f}^{vol} determine the properties of the resulting solution. If the volume flux is the central flux, the high order accurate scheme (2.2) is recovered. If the volume flux is entropy stable or entropy conservative as in (3.3), the resulting scheme (2.5) is entropy stable or entropy conservative, respectively. For instance, the local Lax-Friedrichs flux (LxF)

$$(2.7) \quad \mathbf{f}^{\text{LxF}}(\mathbf{u}_i, \mathbf{u}_j, \hat{\mathbf{n}}_{ij}) = \mathbf{f}^{\text{central}}(\mathbf{u}_i, \mathbf{u}_j, \hat{\mathbf{n}}_{ij}) + \frac{\lambda_{ij}}{2} (\mathbf{u}_i - \mathbf{u}_j),$$

where λ_{ij} is the maximum wavespeed of the 1D Riemann problem with \mathbf{u}_i and \mathbf{u}_j , is a low order, dissipative, entropy stable flux [8, 12, 11, 16].

3. Entropy Stable Finite Difference Methods. Entropy stable schemes are numerical methods which satisfy a form of entropy inequality. The inequality is derived so that a discrete form of the 2nd law of thermodynamics is satisfied by

the scheme. The entropy inequality is a generalization of an energy inequality for nonlinear conservation laws. Assuming admissible quantities, such as positive pressure and density for the compressible Euler equations, a scheme which satisfies a (semi-)discrete entropy inequality typically behaves more robustly. The result is a solution which dissipates mathematical entropy over time, which in some cases is even sufficient to stabilize the solution without relying on heuristic stabilization techniques.

We are particularly interested in equations which satisfy an entropy inequality. The continuous entropy inequality we wish to mimic at the discrete level is:

$$(3.1) \quad \frac{\partial \eta(\mathbf{u})}{\partial t} + \sum_{k=1}^d \frac{\partial F_k(\mathbf{u})}{\partial x_k} \leq 0,$$

where $\eta : \mathbb{R}^v \rightarrow \mathbb{R}$ is called the *entropy function*, and $F_1, \dots, F_d : \mathbb{R}^v \rightarrow \mathbb{R}$ are called the *entropy fluxes*. In particular, we choose η and F_k such that (η, F_k) are a *convex entropy, entropy flux pair*. Here, η is convex, and

$$\frac{\partial F_k}{\partial \mathbf{u}} = \mathbf{v}^T \frac{\partial \mathbf{f}_k(\mathbf{u})}{\partial \mathbf{u}},$$

where $\mathbf{v} = \nabla_{\mathbf{u}} \eta$ are referred to as the *entropy variables*. The *entropy fluxes* F_k are given by

$$(3.2) \quad F_k(\mathbf{u}) = \mathbf{v}^T \mathbf{f}_k(\mathbf{u}) - \psi_k(\mathbf{u}),$$

where $\psi_1, \dots, \psi_d : \mathbb{R}^v \rightarrow \mathbb{R}$ are referred to as the *entropy potentials* [7]. We define an entropy *stable* or *conservative* flux as one which satisfies one of the following properties:

$$(3.3) \quad \begin{aligned} (\mathbf{v}_j - \mathbf{v}_i)^T \mathbf{f}(\mathbf{u}_i, \mathbf{u}_j, \hat{\mathbf{n}}_{ij}) &= (\psi(\mathbf{u}_j) - \psi(\mathbf{u}_i)) \cdot \hat{\mathbf{n}}_{ij} && \text{Entropy Conservative,} \\ (\mathbf{v}_j - \mathbf{v}_i)^T \mathbf{f}(\mathbf{u}_i, \mathbf{u}_j, \hat{\mathbf{n}}_{ij}) &\leq (\psi(\mathbf{u}_j) - \psi(\mathbf{u}_i)) \cdot \hat{\mathbf{n}}_{ij} && \text{Entropy Stable.} \end{aligned}$$

Recall, if a volume flux \mathbf{f}^{vol} is entropy stable, the flux differencing scheme (2.5) satisfies an entropy inequality (3.1). For instance, the scheme (4.1) with entropy stable flux \mathbf{f}^{LxF} satisfies the entropy inequality (3.1).

3.1. Discrete Nodal Entropy Stability. In this section, we will discuss the discretization of a high order accurate (in sufficiently regular regions), conservative, entropy stable scheme of the form:

$$(3.4) \quad \begin{aligned} \mathbf{M} \frac{d\mathbf{u}}{dt} + \mathbf{r} &= \mathbf{0}, \\ \mathbf{r}_i &= \sum_j \|\mathbf{n}_{ij}\| \mathbf{f}_{ij}(\boldsymbol{\theta}_{ij}). \end{aligned}$$

Here, $\boldsymbol{\theta} \geq 0$ are called the *diffusion coefficients*, which parameterize $\mathbf{f}_{ij}(\boldsymbol{\theta}_{ij})$ via

$$(3.5) \quad \mathbf{f}_{ij}(\boldsymbol{\theta}) = \mathbf{f}_{ij}^H + \boldsymbol{\theta}(\mathbf{u}_i - \mathbf{u}_j),$$

where $\mathbf{f}_{ij}^H = \mathbf{f}^{\text{central}}(\mathbf{u}_i, \mathbf{u}_j, \hat{\mathbf{n}}_{ij})$ is the high order accurate central flux. Assuming $\boldsymbol{\theta}_{ij}$ is symmetric, this is equivalent to adding a weighted graph Laplacian term to the formulation through the high order flux. That is, $\boldsymbol{\theta}_{ij}$ is proportional to dissipation introduced into the flux \mathbf{f}_{ij}^H .

We will now discuss a high order accurate (in sufficiently smooth regions) discretization of the entropy inequality (3.1) on node x_i . The chain rule allows us to decompose the time derivative of the entropy function as $\left[\frac{\partial \eta(\mathbf{u})}{\partial t}\right]_{x_i} = (\nabla_{\mathbf{u}} \eta)_{x_i}^T \left(\frac{\partial \mathbf{u}}{\partial t}\right)_{x_i}$. Using this fact, we will discretize the time derivative of the entropy η at x_i by $\mathbf{v}_i^T \frac{d\mathbf{u}_i}{dt}$, where $\mathbf{v} = \mathbf{v}(\mathbf{u})$ consists of pointwise evaluations of the entropy variables. To discretize the spatial derivative of the entropy fluxes, we will apply a flux differencing procedure on the entropy potential relation (3.2) to obtain

$$\begin{aligned} \left[\sum_{k=1}^d \frac{\partial F_k(\mathbf{u})}{\partial x_k}\right]_{x_i} &\approx \frac{1}{\mathbf{M}_{ii}} \sum_j \|\mathbf{n}_{ij}\| (\mathbf{v}_j^T \mathbf{f}_{ij}(\boldsymbol{\theta}_{ij}) - \psi(\mathbf{u}_j) \cdot \hat{\mathbf{n}}_{ij}), \\ (3.6) \quad &= \frac{1}{\mathbf{M}_{ii}} \sum_j \|\mathbf{n}_{ij}\| (\mathbf{v}_j^T \mathbf{f}_{ij}(\boldsymbol{\theta}_{ij}) - (\psi(\mathbf{u}_j) - \psi(\mathbf{u}_i)) \cdot \hat{\mathbf{n}}_{ij}), \end{aligned}$$

where the key step in equation (3.6) is due to the fact that $\mathbf{D}_k \mathbf{1} = \mathbf{0}$. At this point, the entropy inequality (3.1) evaluated at node x_i can be discretized as follows:

$$\begin{aligned} &\mathbf{v}_i^T \frac{d\mathbf{u}_i}{dt} + \frac{1}{\mathbf{M}_{ii}} \sum_j \|\mathbf{n}_{ij}\| (\mathbf{v}_j^T \mathbf{f}_{ij}(\boldsymbol{\theta}_{ij}) - (\psi(\mathbf{u}_j) - \psi(\mathbf{u}_i)) \cdot \hat{\mathbf{n}}_{ij}) \leq 0, \\ (\text{by (3.4)}) \quad &\mathbf{v}_i^T \left(-\frac{1}{\mathbf{M}_{ii}} \sum_j \|\mathbf{n}_{ij}\| \mathbf{f}_{ij}(\boldsymbol{\theta}_{ij})\right) + \frac{1}{\mathbf{M}_{ii}} \sum_j \|\mathbf{n}_{ij}\| (\mathbf{v}_j^T \mathbf{f}_{ij}(\boldsymbol{\theta}_{ij}) - (\psi(\mathbf{u}_j) - \psi(\mathbf{u}_i)) \cdot \hat{\mathbf{n}}_{ij}) \leq 0, \\ (\mathbf{M}_{ii} > 0) \quad &\sum_j \|\mathbf{n}_{ij}\| \left[(\mathbf{v}_j - \mathbf{v}_i)^T \mathbf{f}_{ij}(\boldsymbol{\theta}_{ij}) - (\psi(\mathbf{u}_j) - \psi(\mathbf{u}_i)) \cdot \hat{\mathbf{n}}_{ij}\right] \leq 0. \end{aligned}$$

Then, directly plugging in the definition of $\mathbf{f}_{ij}(\boldsymbol{\theta}_{ij})$ from (3.5), we obtain:

$$\begin{aligned} &\sum_j \|\mathbf{n}_{ij}\| \left[(\mathbf{v}_j - \mathbf{v}_i)^T (\mathbf{f}_{ij}^H + \boldsymbol{\theta}_{ij}(\mathbf{u}_i - \mathbf{u}_j)) - (\psi(\mathbf{u}_j) - \psi(\mathbf{u}_i)) \cdot \hat{\mathbf{n}}_{ij}\right] \leq 0, \\ &\sum_j \|\mathbf{n}_{ij}\| \left[(\mathbf{v}_j - \mathbf{v}_i)^T \mathbf{f}_{ij}^H - (\psi(\mathbf{u}_j) - \psi(\mathbf{u}_i)) \cdot \hat{\mathbf{n}}_{ij}\right] - \sum_j \|\mathbf{n}_{ij}\| \left[(\mathbf{v}_j - \mathbf{v}_i)^T (\mathbf{u}_j - \mathbf{u}_i)\right] \boldsymbol{\theta}_{ij} \leq 0, \\ (3.7) \quad &\mathbf{a}_i^T \boldsymbol{\theta}_i \geq b_i, \end{aligned}$$

where

$$\begin{aligned} (\mathbf{a}_i)_j &= \mathbf{a}_{ij} = \|\mathbf{n}_{ij}\| \left[(\mathbf{v}_j - \mathbf{v}_i)^T (\mathbf{u}_j - \mathbf{u}_i)\right], \\ b_i &= \sum_j \|\mathbf{n}_{ij}\| \left[(\mathbf{v}_j - \mathbf{v}_i)^T \mathbf{f}_{ij}^H - (\psi(\mathbf{u}_j) - \psi(\mathbf{u}_i)) \cdot \hat{\mathbf{n}}_{ij}\right], \end{aligned}$$

and $(\boldsymbol{\theta}_i)_j = \boldsymbol{\theta}_{ij}$. Note in this case, \mathbf{a}_i can be interpreted as the entropy dissipation at node x_i , and b_i as the nodal entropy violation of the high order method at node x_i . That is, $b_i \leq 0$ corresponds to when the high order method satisfies the discrete entropy inequality at node x_i , and $b_i > 0$ corresponds to a violation of the discrete entropy inequality by the high order method.

The discrete entropy inequality (3.7) allows one to determine diffusion coefficients $\boldsymbol{\theta}_{ij}$ such that the resulting scheme (3.4) satisfies the semi-discrete entropy inequality. In the next lemma, we argue that such a discrete entropy inequality is feasible.

LEMMA 3.1. *Assume the finite difference solution \mathbf{u} is admissible, such that η is strictly convex at each \mathbf{u}_i . Then, there exists $\boldsymbol{\theta}_i \geq 0$ such that $\mathbf{a}_i^T \boldsymbol{\theta}_i \geq b_i$.*

Proof. The entropy projection matrix $\left(\frac{d\mathbf{u}}{d\mathbf{v}}\right)_{\mathbf{u}} \in \mathbb{R}^{v \times v}$, evaluated at any admissible intermediate state between \mathbf{u}_i and \mathbf{u}_j , is symmetric positive definite. Therefore, if we consider \mathbf{a}_{ij} :

$$\begin{aligned} \mathbf{a}_{ij} &= \|\mathbf{n}_{ij}\| \left[(\mathbf{v}_j - \mathbf{v}_i)^T (\mathbf{u}_j - \mathbf{u}_i) \right], \\ (\text{chain rule}) \quad &= \|\mathbf{n}_{ij}\| \left[(\mathbf{v}_j - \mathbf{v}_i)^T \left(\frac{d\mathbf{u}}{d\mathbf{v}} \right)_{\mathbf{u}} (\mathbf{v}_j - \mathbf{v}_i) \right], \\ &\geq 0. \end{aligned}$$

In the case where $b_i \leq 0$, $\boldsymbol{\theta}_i = \mathbf{0}$ is feasible for (3.7). Suppose $b_i > 0$. In this case, since b_i is nonzero, there must be some j for which $\|\mathbf{n}_{ij}\| \left[(\mathbf{v}_j - \mathbf{v}_i)^T \mathbf{f}_{ij}^H - (\psi(\mathbf{u}_j) - \psi(\mathbf{u}_i)) \cdot \hat{\mathbf{n}}_{ij} \right] > 0$. Thus, we must also have that $\mathbf{u}_i \neq \mathbf{u}_j$. Therefore, $\mathbf{a}_{ij} > 0$, and so $\mathbf{a}_i \neq \mathbf{0}$. Thus, $\mathbf{a}_i^T \mathbf{a}_i > 0$. Fixing $\lambda = \frac{b_i}{\mathbf{a}_i^T \mathbf{a}_i} > 0$, we see that $\boldsymbol{\theta}_i = \lambda \mathbf{a}_i \geq 0$ satisfies $\mathbf{a}_i^T \boldsymbol{\theta}_i = b_i$. \square

Consider the form of $\mathbf{f}_{ij}(\boldsymbol{\theta}_{ij})$ from (3.5). Recall, $\boldsymbol{\theta}_{ij}$ is proportional to dissipation added to \mathbf{f}_{ij}^H . So, we seek to minimize $\boldsymbol{\theta}_i$ in some sense while ensuring that it satisfies $\mathbf{a}_i^T \boldsymbol{\theta}_i \geq b_i$ and $\boldsymbol{\theta}_i \geq 0$. To do this, we will set the *pre-symmetrized* diffusion coefficients $\hat{\boldsymbol{\theta}}_i$ as the solution to the optimization problem:

$$(3.8) \quad \begin{aligned} &\min \quad \hat{\boldsymbol{\theta}}^T \hat{\boldsymbol{\theta}}. \\ &\mathbf{a}_i^T \hat{\boldsymbol{\theta}} \geq b_i \\ &\hat{\boldsymbol{\theta}} \geq 0 \end{aligned}$$

Note that, in order to preserve conservation (see Section (3.2) for more details), the diffusion coefficients must undergo an additional symmetrization procedure before being applied to the blended scheme (3.4).

The following lemma will show that such a problem has an explicit form for its optimal solution.

LEMMA 3.2. *The problem (3.8) is feasible and has optimal solution $\hat{\boldsymbol{\theta}} = \frac{b_i \mathbf{a}_i}{\mathbf{a}_i^T \mathbf{a}_i}$ if $b_i > 0$, and $\hat{\boldsymbol{\theta}} = \mathbf{0}$ if $b_i \leq 0$.*

Proof. By Lemma (3.1), the optimization problem (3.8) is feasible. If $b_i \leq 0$, then, $\hat{\boldsymbol{\theta}} = \mathbf{0}$ is feasible. Moreover, $\mathbf{0}$ optimizes the objective $\hat{\boldsymbol{\theta}}^T \hat{\boldsymbol{\theta}} = \|\hat{\boldsymbol{\theta}}\|^2$ over its whole domain. Therefore, $\hat{\boldsymbol{\theta}} = \mathbf{0}$ is optimal when $b_i \leq 0$.

Suppose $b_i > 0$. Consider the relaxed form of the optimization problem (3.8):

$$(3.9) \quad \min_{\mathbf{a}_i^T \hat{\boldsymbol{\theta}} \geq b_i} \hat{\boldsymbol{\theta}}^T \hat{\boldsymbol{\theta}}.$$

Such a problem has a well-known explicit solution: $\hat{\boldsymbol{\theta}}_* = \mathbf{a}_i^\dagger b_i = \frac{b_i \mathbf{a}_i}{\mathbf{a}_i^T \mathbf{a}_i}$. Recall from Lemma (3.1) that $\mathbf{a}_i \geq 0$. Therefore, we have that $\hat{\boldsymbol{\theta}}_* \geq 0$. Hence, $\hat{\boldsymbol{\theta}}_*$ is feasible for (3.8). Since it is optimal for the relaxed form (3.9), it also optimizes (3.8). \square

Note that the solution to the optimization problem is cheap to compute. The resulting scheme does not dramatically increase the runtime of standard finite difference methods.

3.2. Ensuring Conservation. In this section, we discuss a slight restriction on the resulting scheme in order to enforce *conservation*. Conservation is an important property for nonlinear conservation laws which ensures that the variables \mathbf{u} remain discretely conserved by our scheme. For periodic boundary conditions, a scheme is called conservative if the discrete volume integral is equal to $\mathbf{0}$:

$$(3.10) \quad \sum_i \mathbf{M}_{ii} \frac{d\mathbf{u}_i}{dt} = \mathbf{0}.$$

We will also show that the resulting scheme with symmetrized diffusion coefficients is provably entropy stable. For the purposes of conservation, we will require that $\boldsymbol{\theta}_{ij} = \boldsymbol{\theta}_{ji}$. This can be obtained by setting the diffusion coefficients $\boldsymbol{\theta}_{ij} = \max \{ \hat{\boldsymbol{\theta}}_{ij}, \hat{\boldsymbol{\theta}}_{ji} \}$ after determining $\hat{\boldsymbol{\theta}}_{ij}$ from (3.8). The next lemma argues that this procedure does not affect the entropy stability of the resulting scheme.

LEMMA 3.3. *The blended scheme (3.4) is entropy stable when applied with the diffusion coefficients $\boldsymbol{\theta}_{ij} = \max \{ \hat{\boldsymbol{\theta}}_{ij}, \hat{\boldsymbol{\theta}}_{ji} \}$.*

Proof. Consider node x_i . Notice that $\boldsymbol{\theta}_{ij} \geq \hat{\boldsymbol{\theta}}_{ij}$ by definition. Therefore, since $\mathbf{a}_i \geq 0$, it must be the case that $\mathbf{a}_i^T \boldsymbol{\theta}_i \geq \mathbf{a}_i^T \hat{\boldsymbol{\theta}}_i \geq b_i$. Therefore, it satisfies (3.7). Hence, the blended scheme is provably entropy stable.

In order to satisfy conservation for periodic boundary conditions, it suffices to show that the discrete volume integral is equal to $\mathbf{0}$. This next lemma will argue that the imposition of symmetry $\boldsymbol{\theta}_{ij} = \boldsymbol{\theta}_{ji}$ is sufficient for conservation in periodic boundary conditions.

LEMMA 3.4. *The blended scheme (3.4) is conservative when applied with the diffusion coefficients $\boldsymbol{\theta}_{ij}$.*

Proof. Note, in the context of periodic boundary conditions, \mathbf{D}_k is skew-symmetric. Thus, $\mathbf{n}_{ij} = -\mathbf{n}_{ji}$. Furthermore, since $\boldsymbol{\theta}_{ij} = \boldsymbol{\theta}_{ji}$ we have from (3.5) that $\mathbf{f}_{ij}(\boldsymbol{\theta}_{ij}) = -\mathbf{f}_{ji}(\boldsymbol{\theta}_{ji})$. Therefore,

$$\begin{aligned} \text{(by (3.4))} \quad \sum_i \mathbf{M}_{ii} \frac{d\mathbf{u}_i}{dt} &= - \sum_i \sum_j \|\mathbf{n}_{ij}\| \mathbf{f}_{ij}(\boldsymbol{\theta}_{ij}), \\ &= \sum_i \sum_j \|\mathbf{n}_{ji}\| \mathbf{f}_{ji}(\boldsymbol{\theta}_{ji}), \\ &= - \sum_i \mathbf{M}_{ii} \frac{d\mathbf{u}_i}{dt}. \end{aligned}$$

Therefore, $\sum_i \mathbf{M}_{ii} \frac{d\mathbf{u}_i}{dt} = \mathbf{0}$. Therefore, by (3.10), the scheme (3.4) is conservative. \square

3.3. Weakly-Enforced Boundary Conditions. In this section, we discuss the arising discretization when enforcing constant-in-time Dirichlet boundary conditions weakly. Note that strong boundary conditions may be enforced as well [19]. In order to do this, we utilize the SBP property that $\mathbf{D}_k + \mathbf{D}_k^T = \mathbf{B}_k$, where \mathbf{B}_k is a diagonal boundary matrix. Recall the flux differencing technique taken in (2). Applying a similar flux differencing technique, we obtain:

$$\begin{aligned}
\sum_{k=1}^d (\mathbf{D}_k \mathbf{f}_k(\mathbf{u}))_i &= \sum_{k=1}^d \sum_j 2\mathbf{D}_{k,ij} \left(\frac{\mathbf{f}_k(\mathbf{u}_i) + \mathbf{f}_k(\mathbf{u}_j)}{2} \right), \\
(3.11) \quad &= \sum_{k=1}^d \sum_j \left(\mathbf{B}_{k,ij} + \mathbf{D}_{k,ij} - \mathbf{D}_{k,ij}^T \right) \cdot \left(\frac{\mathbf{f}(\mathbf{u}_i) + \mathbf{f}(\mathbf{u}_j)}{2} \right), \\
&= \sum_j \|\mathbf{n}_{ij}\| \cdot \left(\frac{\mathbf{f}(\mathbf{u}_i) + \mathbf{f}(\mathbf{u}_j)}{2} \cdot \frac{\mathbf{n}_{ij}}{\|\mathbf{n}_{ij}\|} \right) + \|\mathbf{b}_i\| \left(\mathbf{f}(\mathbf{u}_i) \cdot \frac{\mathbf{b}_i}{\|\mathbf{b}_i\|} \right),
\end{aligned}$$

where $\mathbf{n}_{ij}, \mathbf{b}_i \in \mathbb{R}^d$ such that $\mathbf{n}_{ij,k} = (\mathbf{D}_k - \mathbf{D}_k^T)_{ij}$ and $\mathbf{b}_{i,k} = \mathbf{B}_{k,ii}$ are outward unit normals scaled by the surface quadrature weights and surface Jacobian factor. The relation on (3.11) arises from the property that $2\mathbf{D}_k = \mathbf{B}_k + \mathbf{D}_k - \mathbf{D}_k^T$. Therefore, the high order method (2.5) and the blended scheme (3.4) can alternatively be discretized by

$$(3.12) \quad \mathbf{M} \frac{d\mathbf{u}_i^H}{dt} + \sum_j \|\mathbf{n}_{ij}\| \mathbf{f}_{ij}^H = -\|\mathbf{b}_i\| \left(\mathbf{f}^{\text{surf}} \left(\mathbf{u}_i, \mathbf{u}_i^{\text{BC}}, \frac{\mathbf{b}_i}{\|\mathbf{b}_i\|} \right) \right),$$

$$(3.13) \quad \mathbf{M} \frac{d\mathbf{u}_i}{dt} + \sum_j \|\mathbf{n}_{ij}\| \mathbf{f}_{ij}(\theta_{ij}) = -\|\mathbf{b}_i\| \left(\mathbf{f}^{\text{surf}} \left(\mathbf{u}_i, \mathbf{u}_i^{\text{BC}}, \frac{\mathbf{b}_i}{\|\mathbf{b}_i\|} \right) \right),$$

where \mathbf{f}^{surf} is a chosen surface flux. The choice of the surface flux is arbitrary, but it must be entropy stable, as in (3.3). By applying the same procedure in Section (3.1), one arrives at the alternative formulation of a discrete entropy inequality:

$$(3.14) \quad \|\mathbf{b}_i\| \left(-\mathbf{v}_i^T \mathbf{f}^{\text{surf}} \left(\mathbf{u}_i, \mathbf{u}_i^{\text{BC}}, \frac{\mathbf{b}_i}{\|\mathbf{b}_i\|} \right) - \psi(\mathbf{u}_i) \cdot \frac{\mathbf{b}_i}{\|\mathbf{b}_i\|} \right)$$

$$(3.15) \quad + \sum_j \|\mathbf{n}_{ij}\| \left[(\mathbf{v}_j - \mathbf{v}_i)^T \mathbf{f}_{ij}(\theta_{ij}) - (\psi(\mathbf{u}_j) - \psi(\mathbf{u}_i)) \cdot \hat{\mathbf{n}}_{ij} \right] \leq 0.$$

Under appropriate boundary conditions, the first term (3.14) can be made entropy stable [3, 18]. Therefore, a sufficient condition for semi-discrete entropy stability is the entropy inequality on (3.15). Observe that this inequality is equivalent in form to that in (3.7). That is, satisfying the discrete entropy inequality (3.7) results in an entropy stable scheme, even in the context of weakly enforced boundary conditions.

In the case of nonperiodic boundary conditions, conservation is implied by the discrete volume integral being equal to the discrete surface integral of the flux function:

$$\sum_i \mathbf{M}_{ii} \frac{d\mathbf{u}_i}{dt} = - \sum_i \|\mathbf{b}_i\| \left(\mathbf{f}^{\text{surf}} \left(\mathbf{u}_i, \mathbf{u}_i^{\text{BC}}, \frac{\mathbf{b}_i}{\|\mathbf{b}_i\|} \right) \right).$$

In order to prove the resulting scheme is conservative, it suffices to show that the discrete integral is equal to the boundary integral of the fluxes:

$$\begin{aligned}
&\sum_i \mathbf{M}_{ii} \frac{d\mathbf{u}_i}{dt}, \\
(\text{by (3.4)}) \quad &= - \sum_i \sum_j \|\mathbf{n}_{ij}\| \mathbf{f}_{ij}(\theta_{ij}) - \sum_i \|\mathbf{b}_i\| \left(\mathbf{f}^{\text{surf}} \left(\mathbf{u}_i, \mathbf{u}_i^{\text{BC}}, \frac{\mathbf{b}_i}{\|\mathbf{b}_i\|} \right) \right), \\
(\text{see (3.4)}) \quad &= - \sum_i \|\mathbf{b}_i\| \left(\mathbf{f}^{\text{surf}} \left(\mathbf{u}_i, \mathbf{u}_i^{\text{BC}}, \frac{\mathbf{b}_i}{\|\mathbf{b}_i\|} \right) \right).
\end{aligned}$$

4. Equivalence with Knapsack Limiting and Positivity Preservation.

In this section, we will tie a connection between knapsack limiting and the ECAV-FD scheme, and we will discuss a strategy for enforcing positivity preservation into the proposed scheme. To do this, we will assume that the chosen timestepper is strong stability preserving (SSP). The update of an SSP timestepper can be expressed as a convex combination of forward Euler updates, which combines the benefits of positivity preservation from forward Euler timestepping with low order methods, with the high order time converges of Runge-Kutta methods. Consider the low order method defined as follows:

$$(4.1) \quad \mathbf{M} \frac{d\mathbf{u}^L}{dt} + \mathbf{r}^L = \mathbf{0},$$

$$\mathbf{r}_i^L = \sum_j \|\mathbf{n}_{ij}\| \mathbf{f}_{ij}^L,$$

$$(4.2) \quad \mathbf{f}_{ij}^L = \mathbf{f}^{\text{LxF}} \left(\mathbf{u}_i, \mathbf{u}_j, \frac{\mathbf{n}_{ij}}{\|\mathbf{n}_{ij}\|} \right).$$

In order to enforce constant-in-time Dirichlet boundary conditions, one may replace the right-hand-side with the appropriate boundary term. The resulting low order method is provably positivity preserving for the compressible Euler and Navier-Stokes equations under appropriate choices of the timestep [11]. Notice:

$$(4.3) \quad \begin{aligned} \mathbf{f}_{ij}^L &= \mathbf{f}_{ij}^H + (\mathbf{f}_{ij}^L - \mathbf{f}_{ij}^H), \\ &= \mathbf{f}_{ij}^H + \frac{\lambda_{ij}}{2} (\mathbf{u}_i - \mathbf{u}_j), \\ &= \mathbf{f}_{ij} \left(\frac{\lambda_{ij}}{2} \right), \end{aligned}$$

where λ_{ij} is defined as in (2.7). We can see from the definition above that there exists a set of diffusion coefficients such that the scheme (3.13) is equivalent to the low order scheme (4.1). Furthermore, more generally, we can observe that for $\theta_{ij} \in [0, 1]$:

$$\begin{aligned} \mathbf{f}_{ij} \left(\frac{\lambda_{ij}}{2} \theta_{ij} \right) &= \mathbf{f}_{ij}^H + \frac{\lambda_{ij}}{2} \theta_{ij} (\mathbf{u}_i - \mathbf{u}_j), \\ &= \mathbf{f}_{ij}^H + \theta_{ij} (\mathbf{f}_{ij}^L - \mathbf{f}_{ij}^H), \\ &= (1 - \theta_{ij}) \mathbf{f}_{ij}^H + \theta_{ij} \mathbf{f}_{ij}^L. \end{aligned}$$

That is, $\mathbf{f}_{ij} \left(\frac{\lambda_{ij}}{2} \theta_{ij} \right)$ can be expressed as a convex combination between the low and high order fluxes \mathbf{f}_{ij}^L and \mathbf{f}_{ij}^H . We then define the weighted evaluation of the flux (3.5), $\mathbf{f}_{ij}^{\text{KL}}(\theta_{ij}) = \mathbf{f}_{ij} \left(\frac{\lambda_{ij}}{2} \theta_{ij} \right)$ the *knapsack* blended flux. The use of this knapsack flux in the scheme (3.13) amounts to *knapsack limiting*, which can be used to preserve positivity. *Limiting coefficients* ℓ^c can be derived such that if $\theta_{ij} \in [\ell^c_{ij}, 1]$, the resulting scheme satisfies a *relative positivity condition*:

$$(4.3) \quad \mathbf{u}_i + \Delta t \cdot \frac{d\mathbf{u}_i}{dt} \geq \alpha \left(\mathbf{u}_i + \Delta t \cdot \frac{d\mathbf{u}_i^L}{dt} \right),$$

for some $\alpha \in [0, 1]$. Importantly, it must be the case that $\ell^c_{ij} = \ell^c_{ji}$ to ensure conservation is satisfied. Thus, a symmetrization process must take place after determining

the limiting coefficients from (4.3). The pre-symmetrization diffusion coefficients $\hat{\boldsymbol{\theta}}_{ij}$ may then be determined from the *quadratic knapsack problem*:

$$(4.4) \quad \begin{aligned} & \min_{\hat{\boldsymbol{\theta}}} \quad \hat{\boldsymbol{\theta}}^T \hat{\boldsymbol{\theta}}, \\ & \mathbf{a}_i^T \hat{\boldsymbol{\theta}} \geq b_i \\ & 0 \leq \hat{\boldsymbol{\theta}} \leq 1 - \boldsymbol{\ell}^c_i \end{aligned}$$

where

$$\begin{aligned} (\mathbf{a}_i)_j &= \|\mathbf{n}_{ij}\| \left[(\mathbf{v}_j - \mathbf{v}_i)^T (\mathbf{f}_{ij}^H - \mathbf{f}_{ij}^L) \right], \\ b_i &= \sum_j \|\mathbf{n}_{ij}\| \left[(\mathbf{v}_j - \mathbf{v}_i)^T \mathbf{f}_{ij}^H - (\psi(\mathbf{u}_j) - \psi(\mathbf{u}_i)) \cdot \hat{\mathbf{n}}_{ij} \right] - \mathbf{a}_i^T \boldsymbol{\ell}^c_i, \\ (\boldsymbol{\ell}^c_i)_j &= \boldsymbol{\ell}^c_{ij}. \end{aligned}$$

An efficient, linear-time algorithm for this quadratic knapsack problem was proved in [4]. At this point, symmetrizing the diffusion coefficients to $\boldsymbol{\theta}_{ij} = \max \{ \hat{\boldsymbol{\theta}}_{ij}, \hat{\boldsymbol{\theta}}_{ji} \}$, the scheme (3.13) is provably positivity preserving when applied with the diffusion coefficients $\boldsymbol{\theta}_{ij} + \boldsymbol{\ell}^c_{ij}$.

Note that the use of the Lax-Friedrichs flux for \mathbf{f}^L is not necessary. The low order flux must be entropy stable, in such a way that the scheme (4.1) preserves positivity. For instance, the HLLC flux can be chosen instead. However, in this case, the resulting knapsack limiting flux $\mathbf{f}_{ij}^{\text{KL}}(\boldsymbol{\theta}_{ij})$ is *not* equivalent to a weighted evaluation of the flux (3.5). That being said, the same strategies apply.

5. Numerical Results. In this section, we first analyze the spatial convergence of the proposed artificial viscosity (ECAV-FD) and knapsack limiting (KL-FD) schemes, and examine their solutions on an entropy stability benchmark. Then, we determine the performance of each scheme by timing against a standard finite difference method for a smooth initial condition. We then apply the proposed schemes to various positivity preservation benchmarks. Finally, we examine the solution to various two-dimensional problems.

All simulations utilize the compressible Euler equations. We use various timesteppers throughout this section, including RK4, a 4-stage 4th order method, and SSPRK43, a strong stability preserving (SSP) 4-stage, 3rd order method. We specify for each experiment whether the timesteppers used a fixed or adaptive timestep, which are both implemented in `OrdinaryDiffEq.jl` [14]. Similarly, we use implementations from `Trixi.jl` [15, 17] for all quantities related to the compressible Euler equations. The KL-FD scheme utilizes the HLLC flux [9] for its entropy stable flux \mathbf{f}^L in all simulations. For this reason, we will refer to it as KL-FD-HLLC for clarity.

5.1. Spatial Convergence. In this section, we examine the spatial convergence of the ECAV-FD and KL-FD-HLLC schemes in order to demonstrate that they obtain arbitrarily high spatial orders of accuracy. We also visually examine solutions generated by each scheme.

We start by numerically estimating the spatial convergence of a 1D density wave with a smooth initial condition. Then, we show plots for the Shu-Osher shock tube problem.

First, we test the high order spatial convergence of our schemes using a 1D density wave. The initial condition for the 1D compressible Euler density wave is as follows:

$$p(x, 0) = 1, \quad v(x, 0) = 1.7, \quad \rho(x, 0) = \frac{1}{2} \sin(\pi x) + 1.$$

The density wave solution is computed using the RK4 timestepper with a fixed $\Delta t = 10^{-4}$ to a final time of $T = 1$, over the periodic domain $[-1, 1]$. In Tables (1) and (2), the L^2 norm of the solution at the final time is computed against the analytical solution for various node counts n . This is done for polynomial orders $N = 2$ through $N = 5$. The errors are used to estimate the spatial order of convergence. We observe that the optimal order of convergence $\mathcal{O}(\Delta x^N)$ is attained by each scheme.

	$N = 2$		$N = 3$		$N = 4$		$N = 5$	
n	L^2 Error	Rate	L^2 Error	Rate	L^2 Error	Rate	L^2 Error	Rate
16	$1.65 \cdot 10^{-1}$	—	$1.59 \cdot 10^{-2}$	—	$1.59 \cdot 10^{-2}$	—	$6.43 \cdot 10^{-3}$	—
32	$4.18 \cdot 10^{-2}$	1.98	$2.20 \cdot 10^{-3}$	2.86	$2.20 \cdot 10^{-3}$	2.86	$4.99 \cdot 10^{-4}$	3.69
64	$1.05 \cdot 10^{-2}$	2.00	$2.53 \cdot 10^{-4}$	3.12	$2.53 \cdot 10^{-4}$	3.12	$1.87 \cdot 10^{-5}$	4.74
128	$2.62 \cdot 10^{-3}$	2.00	$2.11 \cdot 10^{-5}$	3.58	$2.11 \cdot 10^{-5}$	3.58	$4.43 \cdot 10^{-7}$	5.40
256	$6.56 \cdot 10^{-4}$	2.00	$1.69 \cdot 10^{-6}$	3.64	$1.69 \cdot 10^{-6}$	3.64	$9.41 \cdot 10^{-9}$	5.56
512	$1.64 \cdot 10^{-4}$	2.00	$1.33 \cdot 10^{-7}$	3.67	$1.33 \cdot 10^{-7}$	3.67	$1.78 \cdot 10^{-10}$	5.72

Table 1: Errors and estimated orders of convergence of ECAV-FD for degrees N .

	$N = 2$		$N = 3$		$N = 4$		$N = 5$	
n	L^2 Error	Rate	L^2 Error	Rate	L^2 Error	Rate	L^2 Error	Rate
16	$1.65 \cdot 10^{-1}$	—	$1.59 \cdot 10^{-2}$	—	$1.59 \cdot 10^{-2}$	—	$6.43 \cdot 10^{-3}$	—
32	$4.18 \cdot 10^{-2}$	1.98	$2.20 \cdot 10^{-3}$	2.86	$2.20 \cdot 10^{-3}$	2.86	$4.99 \cdot 10^{-4}$	3.69
64	$1.05 \cdot 10^{-2}$	2.00	$2.53 \cdot 10^{-4}$	3.12	$2.53 \cdot 10^{-4}$	3.12	$1.87 \cdot 10^{-5}$	4.74
128	$2.62 \cdot 10^{-3}$	2.00	$2.11 \cdot 10^{-5}$	3.58	$2.11 \cdot 10^{-5}$	3.58	$4.43 \cdot 10^{-7}$	5.40
256	$6.56 \cdot 10^{-4}$	2.00	$1.69 \cdot 10^{-6}$	3.64	$1.69 \cdot 10^{-6}$	3.64	$9.41 \cdot 10^{-9}$	5.56
512	$1.64 \cdot 10^{-4}$	2.00	$1.35 \cdot 10^{-7}$	3.64	$1.35 \cdot 10^{-7}$	3.64	$1.78 \cdot 10^{-10}$	5.72

Table 2: Errors and estimated orders of convergence of KL-FD-HLLC for degrees N .

5.2. Shu-Osher Shock Tube. Next, we examine the solutions generated in the case when some form of stabilization is required to avoid crashing. To do this, we use the Shu-Osher shock tube initial condition for the 1D compressible Euler equations:

$$(\rho(x, 0), v(x, 0), p(x, 0)) = \begin{cases} (3.857143, 2.629369, 10.3333) & x < -4 \\ (1 + .2 \sin(5x), 0, 1) & \text{otherwise.} \end{cases}$$

The Shu-Osher solution is computed using the adaptive SSPRK43 timestepper, with the absolute and relative tolerances set to 10^{-6} and 10^{-4} respectively. The simulation is performed to a final time of $T = 1.8$, over the domain $[-5, 5]$, with Dirichlet boundary conditions enforcing that the solution remain constant at the boundaries over time. In Figure (1), the density of the solutions at the final time computed using 4th order ECAV-FD and KL-FD-HLLC for $n = 500$ and $n = 1500$ are shown. These node counts are chosen for consistency with [13]. Each solution is compared with a reference solution computed using a 5th order WENO method with 25000 nodes. We observe that for $n = 500$, KL-FD-HLLC is a closer approximation of the reference solution near the highly oscillatory region to the right. We also observe that to the left side, each finite difference approximation has small oscillations. However, for $n = 1500$, we observe that the oscillations are reduced to the left hand side for each

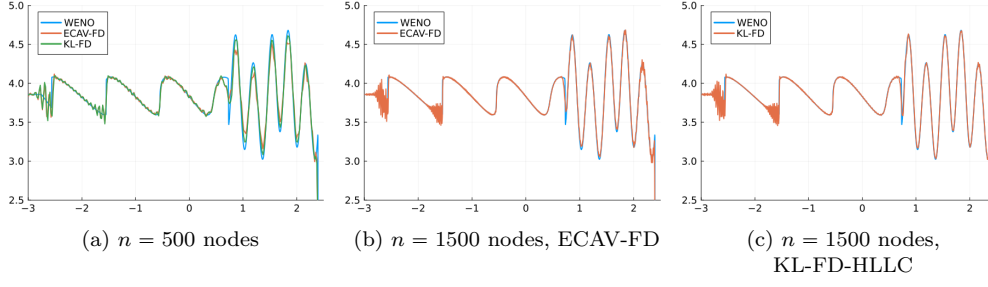


Fig. 1: Density of the Shu-Osher shock tube solution at final time $T = 1.8$ with $N = 4$.

finite difference approximation, and we observe that each finite difference solution is a good approximation of the reference solution on the right hand side.

5.3. Positivity Preservation. In the simulations performed thus far, preservation of positivity was not strictly necessary. Thus, the limiting coefficients ℓ^c were set to $\mathbf{0}$. In this section, we benchmark KL-FD-HLLC in various difficult benchmarks of positivity preservation. Limiting coefficients are set on a nodewise basis, and then symmetrized, via the following formula, in order to satisfy the relative positivity constraint (4.3):

$$(5.1) \quad \hat{\ell}_i^c = \begin{cases} 1 - \frac{(1-\alpha)}{\Delta t} \left(\frac{\mathbf{M}_{ii}\mathbf{u}_i - \Delta t \cdot \mathbf{r}_i^L}{\mathbf{r}_i^H - \mathbf{r}_i^L} \right) & \mathbf{r}_i^H - \mathbf{r}_i^L > 0 \\ 0 & \text{otherwise} \end{cases}, \quad \ell_{ij}^c = \max \left\{ \hat{\ell}_i^c, \hat{\ell}_j^c \right\}.$$

The diffusion coefficients are then determined via the strategy described in (8.2). In this section, we test KL-FD-HLLC in various difficult simulations, often used to test positivity preservation methods.

First, we test KL-FD-HLLC on the 1D compressible Euler, Leblanc shock tube problem. This problem mimics pressure waves in near vacuum conditions, common in hypersonic flow. The initial condition for this problem is as follows:

$$p(x, 0) = \begin{cases} 10^9 & x < 0 \\ 1 & \text{otherwise} \end{cases}, \quad v(x, 0) = 0, \quad \rho(x, 0) = \begin{cases} 2 & x < 0 \\ 10^{-3} & \text{otherwise} \end{cases}.$$

The initial condition has a pressure ratio of 10^9 and a density ratio of 2000. Due to oscillations formed around shocks in high order simulations which are proportional to the jump, preservation of positivity is necessary to produce a stable solution. The Leblanc shock tube solution is computed with the **SSPRK43** timestepper using a fixed timestep of $\Delta t = 6 \cdot 10^{-8}$. This timestep is within 10^{-8} of the maximum stable timestep for the order $N = 6$ simulation. The simulation is performed to a final time of $T = 10^{-4}$, over the domain $[-10, 10]$, with Dirichlet boundary conditions, enforcing that the solution remain constant at the boundaries over time.

In Figure (2), we plot the density, velocity, and pressure of the solution generated by KL-FD-HLLC with 4000 nodes, against a reference solution. The relative positivity constraint with $\alpha = .5$ is enforced. The reference solution is modified from the solution generated by the discontinuous Galerkin version of quadratic knapsack limiting [4], with 3rd order accuracy, and 12000 elements. The plots are shown for both orders

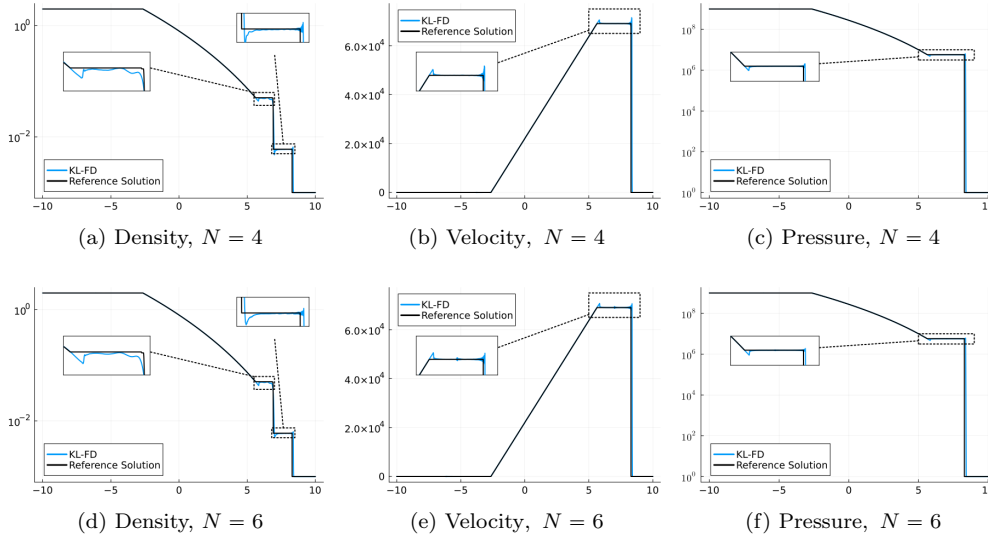


Fig. 2: KL-FD-HLLC solution to the Leblanc shock tube with 4000 nodes and relative positivity constraint $\alpha = .5$.

$N = 4$ and $N = 6$ order accuracy. We observe that the solutions are virtually identical, though there is a slight amount of oscillation present in the velocity of the $N = 6$ solution at the peak. However, this tends not to appear with a smaller chosen timestep.

Next, we test KL-FD-HLLC on the Woodward-Colella blast wave. This problem mimics the interaction of two blast waves, also common in hypersonic flow. The initial condition for this problem is as follows:

$$\rho(x, 0) = 1, \quad v(x, 0) = 0, \quad p(x, 0) = \begin{cases} 10^3 & x < .1 \\ 10^{-2} & .1 \leq x < .9 \\ 10^2 & x \geq .9 \end{cases}.$$

The initial condition has a pressure ratio of 10^5 at the left interface, and 10^4 at the right interface, again making preservation of positivity necessary for a stable simulation. The Woodward-Colella blast wave solution is computed using the **SSPRK43** timestepper with a fixed timestep of $\Delta t = 2 \cdot 10^{-5}$. This timestep is within 10^{-5} of the maximum stable timestep for the order $N = 6$ simulation. The simulation is performed to a final time of $T = .038$, over the domain $[0, 1]$, with reflective boundary conditions.

In Figure (3), we plot the density of the solution generated by KL-FD-HLLC with the HLLC flux with 1200 nodes, against a reference solution. The relative positivity constraint with $\alpha = .1$ is enforced. The reference solution is modified from the solution generated by the low order method (4.1) with a 4th order stencil and 25000 nodes. The plots are shown for both orders $N = 4$ and $N = 6$ order accuracy. We observe that the solutions are similar, but the order $N = 6$ simulation is a bit more dissipative. This is likely partially due to the fact that the limiting coefficients, as obtained in (5.1), must be made larger to account for a wider stencil in the symmetrization process.

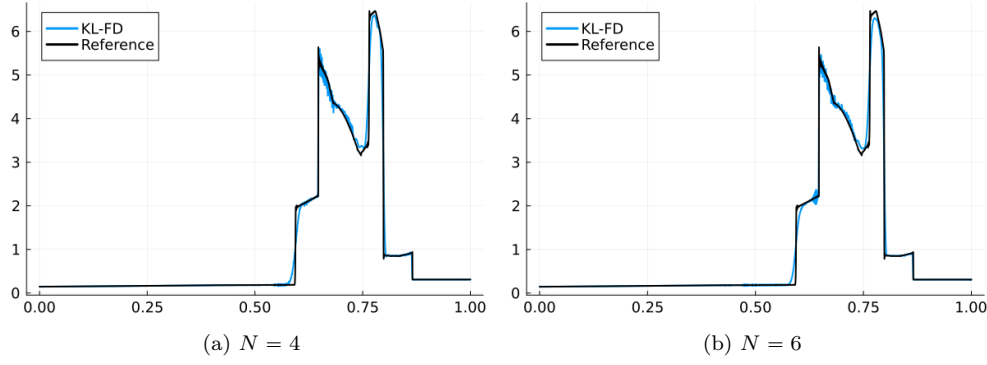


Fig. 3: KL-FD-HLLC solution to the Woodward-Colella blast wave with 1200 nodes and relative positivity constraint $\alpha = .1$.

5.4. Two-Dimensional Solutions. In this section, we test ECAV-FD and KL-FD-HLLC in two dimensional simulations. In particular, we examine the density arising from the Kelvin-Helmholtz instability problem (KHI). This problem is often used to test the behavior of 2D numerical methods in the presence of turbulent-like flow. Without enforcing positivity, collocation-type entropy stable methods tend to crash with negative density for KHI around $T \approx 3.5$ [2]. However, both ECAV-FD and KL-FD-HLLC appear to be able to simulate KHI until and past $T = 25$ without enforcing positivity. In this case, we call this *long-time* Kelvin-Helmholtz instability. The initial condition for KHI is:

$$\begin{aligned} \rho(x, y, 0) &= \frac{1}{2} + \frac{3}{4}B, & v_1(x, y, 0) &= \frac{1}{2}(B - 1), \\ v_2(x, y, 0) &= \frac{1}{10} \sin(2\pi x), & p(x, y, 0) &= 1, \end{aligned}$$

where $B = \tanh(15y + 7.5) - \tanh(15y - 7.5)$. The long-time KHI solution is computed on the periodic domain $[-1, 1]^2$ to a final time $T = 25$, using the adaptive SSPRK43 timestepper, with an absolute tolerance of 10^{-6} and relative tolerance of 10^{-4} . In Figures (4) and (5), we plot the solutions generated by ECAV-FD and KL-FD-HLLC respectively, at times $t = 5$, $t = 10$, and $t = 25$, each for orders $N = 4$ and $N = 6$, and each with 512 nodes along each dimension. The color range was truncated to $[-.25, 2.5]$.

6. Conclusion. In this work, we proposed two approaches for constructing high order accurate, conservative, entropy stable finite difference methods. The first is an entropy correction artificial viscosity method, which introduces a minimal amount of artificial viscosity in order to satisfy a semi-discrete entropy inequality. The second is a knapsack limiting technique, which minimally blends a low order method into a high order method in order to satisfy the same semi-discrete entropy inequality. We also discussed how knapsack limiting can be expressed as a weighted form of the entropy correction artificial viscosity method. Furthermore, knapsack limiting schemes can be used to preserve positivity. We also discussed how weakly-enforced boundary conditions can be imposed using summation by parts finite difference operators. Each scheme exhibits high order accuracy for sufficiently regular solutions, while also

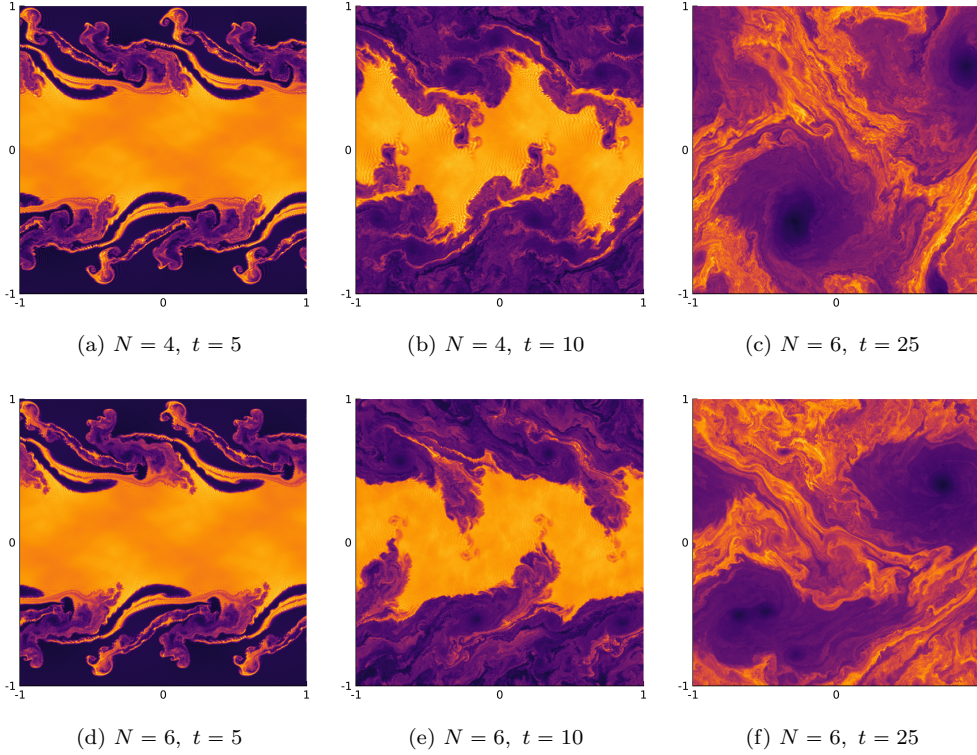


Fig. 4: ECAV-FD solution to Kelvin-Helmholtz instability problem.

retaining entropy stability and conservation.

7. Acknowledgements. The authors gratefully acknowledge helpful discussions with Ayaboe Edoh and Brad Maeng, as well as support from National Science Foundation awards DMS-1943186 and DMS-223148.

8. Appendix: Optimization-Based Relaxation of the Entropy Inequality. In this section, we will discuss a strategy of decoupling the diffusion coefficients in the spatial derivative of the flux and the spatial derivative of the entropy flux. The strategy allows for the artificial diffusion of the spatial derivative of the entropy flux to be decoupled from the diffusion applied to \mathbf{r} from the diffusion coefficients. In effect, this results in a relaxation of the entropy inequality (3.7). It does this by applying only a slight increase in the dimension of the optimization problems (3.8) and (8.2), which does not scale with spatial dimension.

We will demonstrate in the corresponding numerical results section that the ECAV-FD and KL-FD schemes result in excessive dissipation in high orders, and the relaxation discussed in this section helps to recover it. However, we will also show that relaxing the entropy inequality results in more oscillations in the generated solutions. Furthermore, relaxing the entropy inequality too much may result in an unstable scheme. The resulting strategy will be derived for the entropy correction artificial viscosity scheme, but the strategy for the knapsack limiting scheme will also

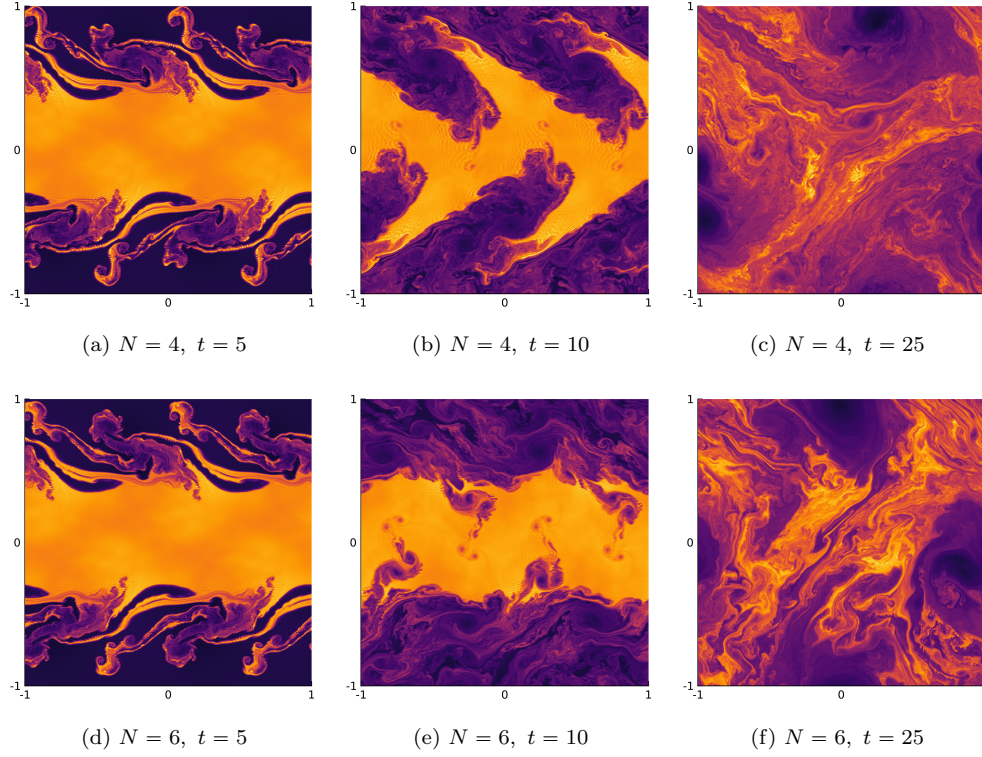


Fig. 5: KL-FD-HLLC solution to Kelvin-Helmholtz instability problem.

be shown. Recall, the spatial derivative of the entropy flux is discretized as follows:

$$\left[\sum_{k=1}^d \frac{\partial F_k(\mathbf{u})}{\partial x_k} \right]_{x_i} \approx \frac{1}{\mathbf{M}_{ii}} \sum_j \|\mathbf{n}_{ij}\| (\mathbf{v}_j^T \mathbf{f}_{ij}(\boldsymbol{\theta}_{ij}) - (\psi(\mathbf{u}_j) - \psi(\mathbf{u}_i)) \cdot \hat{\mathbf{n}}_{ij}).$$

The diffusion coefficients $\boldsymbol{\theta}_{ij}$, which apply diffusion within the flux $\mathbf{f}_{ij}(\boldsymbol{\theta}_{ij})$ to determine \mathbf{r} as in (3.4), also apply diffusion to the spatial derivative of the entropy flux. However, this does not need to be the case. Rather, we can instead replace $\boldsymbol{\theta}_{ij}$ in the discretization of the spatial derivative of the entropy flux with an additional free variable, as such:

$$\left[\sum_{k=1}^d \frac{\partial F_k(\mathbf{u})}{\partial x_k} \right]_{x_i} \approx \frac{1}{\mathbf{M}_{ii}} \sum_j \|\mathbf{n}_{ij}\| (\mathbf{v}_j^T \mathbf{f}_{ij}(\boldsymbol{\tau}_i) - (\psi(\mathbf{u}_j) - \psi(\mathbf{u}_i)) \cdot \hat{\mathbf{n}}_{ij}),$$

where $\boldsymbol{\tau} \in \mathbb{R}^n$. At this point, the discretization of the entropy inequality (3.1) has a

new form:

$$\begin{aligned}
& \mathbf{v}_i^T \frac{d\mathbf{u}_i}{dt} + \frac{1}{\mathbf{M}_{ii}} \sum_j \|\mathbf{n}_{ij}\| (\mathbf{v}_j^T \mathbf{f}_{ij}(\boldsymbol{\tau}_i) - (\psi(\mathbf{u}_j) - \psi(\mathbf{u}_i)) \cdot \hat{\mathbf{n}}_{ij}) \leq 0, \\
& \text{(by (3.4))} \\
& \mathbf{v}_i^T \left(-\frac{1}{\mathbf{M}_{ii}} \sum_j \|\mathbf{n}_{ij}\| \mathbf{f}_{ij}(\boldsymbol{\theta}_{ij}) \right) + \frac{1}{\mathbf{M}_{ii}} \sum_j \|\mathbf{n}_{ij}\| (\mathbf{v}_j^T \mathbf{f}_{ij}(\boldsymbol{\tau}_i) - (\psi(\mathbf{u}_j) - \psi(\mathbf{u}_i)) \cdot \hat{\mathbf{n}}_{ij}) \leq 0, \\
& (\mathbf{M}_{ii} > 0) \quad \sum_j \|\mathbf{n}_{ij}\| [(\mathbf{v}_j^T \mathbf{f}_{ij}(\boldsymbol{\tau}_i) - \mathbf{v}_i^T \mathbf{f}_{ij}(\boldsymbol{\theta}_{ij})) - (\psi(\mathbf{u}_j) - \psi(\mathbf{u}_i)) \cdot \hat{\mathbf{n}}_{ij}] \leq 0, \\
& \quad - \sum_j \|\mathbf{n}_{ij}\| [(\mathbf{v}_j - \mathbf{v}_i)^T \mathbf{f}_{ij}^H - (\psi(\mathbf{u}_j) - \psi(\mathbf{u}_i)) \cdot \hat{\mathbf{n}}_{ij}] \\
& \quad + \sum_j \|\mathbf{n}_{ij}\| [\mathbf{v}_i^T (\mathbf{u}_i - \mathbf{u}_j)] \boldsymbol{\theta}_{ij} - \sum_j \|\mathbf{n}_{ij}\| [\mathbf{v}_j^T (\mathbf{u}_i - \mathbf{u}_j)] \boldsymbol{\tau}_i \geq 0, \\
& \quad \mathbf{a}_i^T \begin{bmatrix} \boldsymbol{\theta}_i \\ \boldsymbol{\tau}_i \end{bmatrix} \geq b_i,
\end{aligned}$$

where

$$\begin{aligned}
(\mathbf{a}_i)_j = \mathbf{a}_{ij} &= \begin{cases} \|\mathbf{n}_{ij}\| [\mathbf{v}_i^T (\mathbf{u}_i - \mathbf{u}_j)] & j = \text{end} \\ -\sum_j \|\mathbf{n}_{ij}\| [\mathbf{v}_j^T (\mathbf{u}_i - \mathbf{u}_j)] & \text{otherwise} \end{cases}, \\
b_i &= \sum_j \|\mathbf{n}_{ij}\| [(\mathbf{v}_j - \mathbf{v}_i)^T \mathbf{f}_{ij}^H - (\psi(\mathbf{u}_j) - \psi(\mathbf{u}_i)) \cdot \hat{\mathbf{n}}_{ij}].
\end{aligned}$$

We call this the *relaxed entropy inequality*. Then, the pre-symmetrized diffusion coefficients and $\boldsymbol{\tau}$ -coefficients can be determined through the same optimization problem as before:

$$(8.1) \quad \begin{aligned} & \min_{\substack{\hat{\boldsymbol{\theta}} \\ \hat{\boldsymbol{\tau}}}} \begin{bmatrix} \hat{\boldsymbol{\theta}} \\ \hat{\boldsymbol{\tau}} \end{bmatrix}^T \begin{bmatrix} \hat{\boldsymbol{\theta}} \\ \hat{\boldsymbol{\tau}} \end{bmatrix} \\ & \mathbf{a}_i^T \begin{bmatrix} \hat{\boldsymbol{\theta}} \\ \hat{\boldsymbol{\tau}} \end{bmatrix} \geq b_i \\ & \hat{\boldsymbol{\theta}} \geq 0 \\ & \hat{\boldsymbol{\tau}} \geq 0 \end{aligned}$$

We note that the property $\mathbf{a}_i \geq 0$ is lost in this strategy. However, the above problem still yields an explicit solution. Note, it can be rewritten with elementwise upper bounds. Specifically, it is equivalent when given the constraint $0 \leq \hat{\boldsymbol{\theta}} \leq \infty$. It is shown in [4] that Algorithm 3.1 converges in exactly one iteration to the solution for such a problem. Therefore, an explicit formula can be derived for the optimal solution for the optimization problem (8.1):

$$\mathbf{a}_{ij}^c = \begin{cases} \mathbf{a}_{ij} & \mathbf{a}_{ij} \geq 0 \\ 0 & \text{otherwise} \end{cases}, \quad \begin{bmatrix} \hat{\boldsymbol{\theta}}_i \\ \hat{\boldsymbol{\tau}}_i \end{bmatrix} = \frac{b_i \mathbf{a}_i^c}{\mathbf{a}_i^T \mathbf{a}_i^c}.$$

Note that since each $\boldsymbol{\tau}$ -coefficient is unique to each node and does not apply diffusion to \mathbf{r} , no symmetrization is needed for the $\boldsymbol{\tau}$ -coefficients: just for the diffusion coefficients.

This strategy of relaxing the entropy inequality can also be applied to knapsack limiting. In which case, the resulting vector \mathbf{a}_i and scalar b_i have the following form:

$$(\mathbf{a}_i)_j = \mathbf{a}_{ij} = \begin{cases} \|\mathbf{n}_{ij}\| [\mathbf{v}_i^T (\mathbf{f}_{ij}^L - \mathbf{f}_{ij}^H)] & j = \text{end} \\ -\sum_j \|\mathbf{n}_{ij}\| [\mathbf{v}_j^T (\mathbf{f}_{ij}^L - \mathbf{f}_{ij}^H)] & \text{otherwise} \end{cases},$$

$$b_i = \sum_j \|\mathbf{n}_{ij}\| \left[(\mathbf{v}_j - \mathbf{v}_i)^T \mathbf{f}_{ij}^H - (\psi(\mathbf{u}_j) - \psi(\mathbf{u}_i)) \cdot \hat{\mathbf{n}}_{ij} \right].$$

Then, the pre-symmetrization diffusion coefficients can be determined through the same quadratic continuous knapsack problem:

$$(8.2) \quad \begin{aligned} & \min_{\begin{bmatrix} \hat{\boldsymbol{\theta}} \\ \tau \end{bmatrix}} \begin{bmatrix} \hat{\boldsymbol{\theta}} \\ \tau \end{bmatrix}^T \begin{bmatrix} \hat{\boldsymbol{\theta}} \\ \tau \end{bmatrix} \\ & \mathbf{a}_i^T \begin{bmatrix} \hat{\boldsymbol{\theta}} \\ \tau \end{bmatrix} \geq b_i \\ & 0 \leq \hat{\boldsymbol{\theta}} \leq 1 - \ell^{\mathbf{c}_i} \\ & 0 \leq \tau \leq 1 \end{aligned}$$

8.1. Relaxed Entropy Inequality Numerical Results. In this section, we revisit the numerical experiments done in Section (5) with the relaxed versions of ECAV-FD and KL-FD-HLLC. We will refer to each scheme as RECAV-FD and RKL-FD-HLLC respectively. We will demonstrate that the ECAV-FD and KL-FD schemes result in excessive dissipation in high orders, while RECAV-FD and RKL-FD-HLLC help to recover it. However, we will also show that RECAV-FD and RKL-FD-HLLC result in more oscillations in the generated solutions.

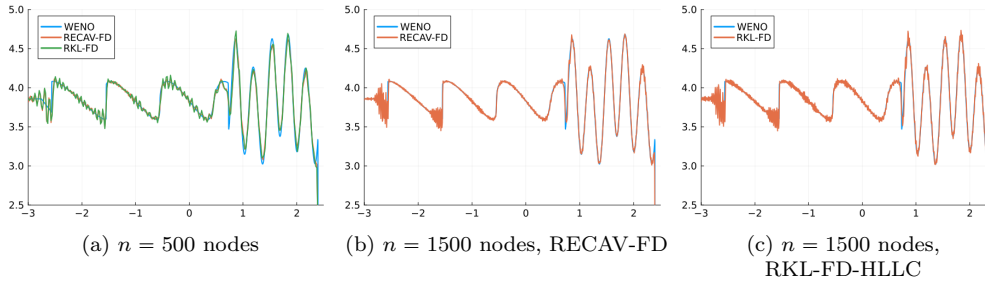
First, we perform the same convergence experiments to analyze the order of spatial convergence of the relaxed schemes. In Tables (3) and (4), the L^2 norm of the solution at the final time is computed against the analytical solution for various node counts n . This is done for polynomial orders $N = 2$ through $N = 5$. The errors are again used to estimate the spatial order of convergence. We observe that the optimal order of convergence $\mathcal{O}(\Delta x^N)$ is attained by each scheme. Moreover, we observe that for odd N , the errors exhibits an improved order $\mathcal{O}(\Delta x^{N+1})$ convergence.

	$N = 2$		$N = 3$		$N = 4$		$N = 5$	
n	L^2 Error	Rate	L^2 Error	Rate	L^2 Error	Rate	L^2 Error	Rate
16	$1.65 \cdot 10^{-1}$	—	$6.28 \cdot 10^{-3}$	—	$6.28 \cdot 10^{-3}$	—	$1.81 \cdot 10^{-3}$	—
32	$4.16 \cdot 10^{-2}$	1.99	$4.36 \cdot 10^{-4}$	3.85	$4.36 \cdot 10^{-4}$	3.85	$7.02 \cdot 10^{-5}$	4.69
64	$1.05 \cdot 10^{-2}$	1.99	$2.53 \cdot 10^{-5}$	4.11	$2.53 \cdot 10^{-5}$	4.11	$1.13 \cdot 10^{-6}$	5.95
128	$2.62 \cdot 10^{-3}$	2.00	$1.37 \cdot 10^{-6}$	4.20	$1.37 \cdot 10^{-6}$	4.20	$1.06 \cdot 10^{-8}$	6.74
256	$6.55 \cdot 10^{-4}$	2.00	$8.08 \cdot 10^{-8}$	4.09	$8.08 \cdot 10^{-8}$	4.09	$8.35 \cdot 10^{-11}$	6.99
512	$1.64 \cdot 10^{-4}$	2.00	$4.97 \cdot 10^{-9}$	4.02	$4.97 \cdot 10^{-9}$	4.02	$8.54 \cdot 10^{-13}$	6.61

Table 3: Errors and estimated orders of convergence of RECAV-FD for degrees N .

Now, we examine the behavior of the relaxed schemes in the Sod shocktube problem. In Figure (6), we plot the solution to the Sod shocktube problem using each relaxed scheme. We observe that the relaxed versions of each scheme tend to generate more oscillatory solutions, compared against their unrelaxed versions, whose solutions are shown in Figure (1). However, we observe that for $n = 500$, each relaxed scheme does a better job approximating the highly oscillatory region to the right.

	$N = 2$		$N = 3$		$N = 4$		$N = 5$	
n	L^2 Error	Rate	L^2 Error	Rate	L^2 Error	Rate	L^2 Error	Rate
16	$1.65 \cdot 10^{-1}$	—	$7.05 \cdot 10^{-3}$	—	$7.05 \cdot 10^{-3}$	—	$2.74 \cdot 10^{-3}$	—
32	$4.16 \cdot 10^{-2}$	1.99	$5.42 \cdot 10^{-4}$	3.70	$5.42 \cdot 10^{-4}$	3.70	$1.17 \cdot 10^{-4}$	4.55
64	$1.04 \cdot 10^{-2}$	1.99	$3.07 \cdot 10^{-5}$	4.14	$3.07 \cdot 10^{-5}$	4.14	$1.82 \cdot 10^{-6}$	6.01
128	$2.62 \cdot 10^{-3}$	2.00	$1.53 \cdot 10^{-6}$	4.33	$1.53 \cdot 10^{-6}$	4.33	$1.73 \cdot 10^{-8}$	6.72
256	$6.55 \cdot 10^{-4}$	2.00	$8.42 \cdot 10^{-8}$	4.18	$8.42 \cdot 10^{-8}$	4.18	$1.44 \cdot 10^{-10}$	6.91
512	$1.64 \cdot 10^{-4}$	2.00	$5.03 \cdot 10^{-9}$	4.07	$5.03 \cdot 10^{-9}$	4.07	$1.41 \cdot 10^{-12}$	6.67

Table 4: Errors and estimated orders of convergence of RKL-HLLC-FD for degrees N .Fig. 6: Density of the Shu-Osher shock tube solution at final time $T = 1.8$ with $N = 4$.

In Figure (7), we show the same plots, but this time with a 6th order approximation. We observe that the solutions generated by the original, unrelaxed schemes are more dissipative than the solutions in Figure (1). We also again observe that for $n = 500$, each relaxed scheme does a better job approximating the highly oscillatory region to the right. However, the solutions generated by the relaxed schemes RECAV-FD and RKL-FD appear more oscillatory. We observe this behavior in general.

REFERENCES

- [1] Jesse Chan. An artificial viscosity approach to high order entropy stable discontinuous Galerkin methods. *arXiv preprint arXiv:2501.16529*, 2025.
- [2] Jesse Chan, Hendrik Ranocha, Andrés M. Rueda-Ramírez, Gregor Gassner, and Tim Warburton. On the Entropy Projection and the Robustness of High Order Entropy Stable Discontinuous Galerkin Schemes for Under-Resolved Flows. *Frontiers in Physics*, Volume 10 - 2022, 2022.
- [3] Tianheng Chen and Chi-Wang Shu. Entropy stable high order discontinuous Galerkin methods with suitable quadrature rules for hyperbolic conservation laws. *Journal of Computational Physics*, 345:427–461, 2017.
- [4] Brian Christner and Jesse Chan. Entropy stable nodal discontinuous Galerkin methods via quadratic knapsack limiting. *arXiv preprint arXiv:2507.14488*, 2025.
- [5] Travis C Fisher and Mark H Carpenter. High-order entropy stable finite difference schemes for nonlinear conservation laws: Finite domains. *Journal of Computational Physics*, 252:518–557, 2013.
- [6] Gregor J. Gassner, Andrew R. Winters, and David A. Kopriva. Split form nodal discontinuous Galerkin schemes with summation-by-parts property for the compressible Euler equations. *Journal of Computational Physics*, 327:39–66, 2016.
- [7] Edwige Godlewski and Pierre-Arnaud Raviart. *Numerical approximation of hyperbolic systems of conservation laws*, volume 118. Springer Science & Business Media, 2013.

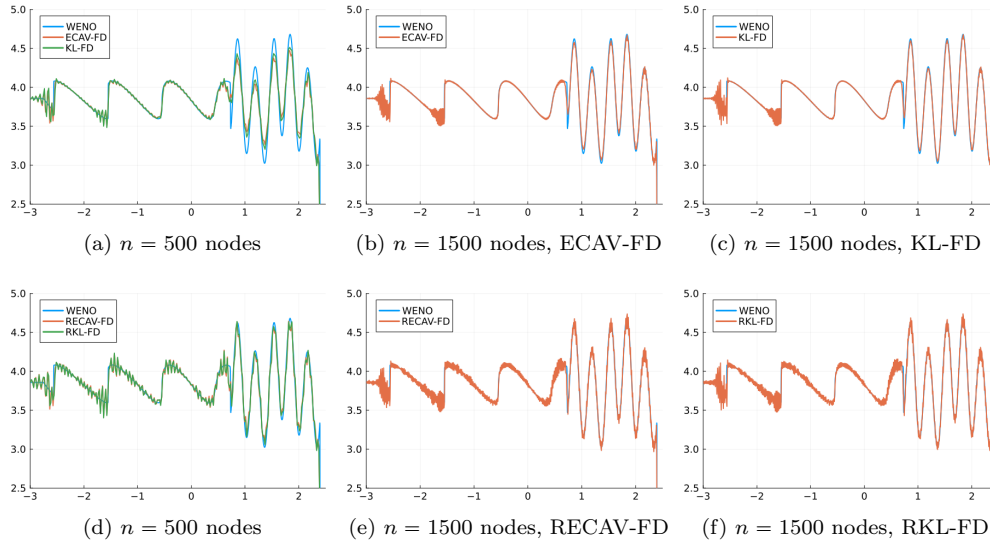


Fig. 7: Density of the Shu-Osher shock tube solution at final time $T = 1.8$ with $N = 6$.

- [8] Jean-Luc Guermond, Bojan Popov, and Ignacio Tomas. Invariant domain preserving discretization-independent schemes and convex limiting for hyperbolic systems. *Computer Methods in Applied Mechanics and Engineering*, 347:143–175, 2019.
- [9] Amiram Harten, Peter D. Lax, and Bram van Leer. On Upstream Differencing and Godunov-Type Schemes for Hyperbolic Conservation Laws. *SIAM Review*, 25(1):35–61, 1983.
- [10] Yimin Lin and Jesse Chan. High order entropy stable discontinuous Galerkin spectral element methods through subcell limiting. *Journal of Computational Physics*, 498:112677, 2024.
- [11] Yimin Lin, Jesse Chan, and Ignacio Tomas. A positivity preserving strategy for entropy stable discontinuous Galerkin discretizations of the compressible Euler and Navier-Stokes equations. *Journal of Computational Physics*, 475:111850, 2023.
- [12] Will Pazner. Sparse invariant domain preserving discontinuous Galerkin methods with subcell convex limiting. *Computer Methods in Applied Mechanics and Engineering*, 382:113876, 2021.
- [13] Andrius Popovas. DISPATCH methods: An approximate, entropy-based Riemann solver for ideal magnetohydrodynamics. *Astronomy Astrophysics*, 698:A69, June 2025.
- [14] Christopher Rackauckas and Qing Nie. DifferentialEquations.jl – A Performant and Feature-Rich Ecosystem for Solving Differential Equations in Julia. *The Journal of Open Research Software*, 5(1), 2017. Exported from <https://app.dimensions.ai> on 2019/05/05.
- [15] Hendrik Ranocha, Michael Schlottke-Lakemper, Andrew Ross Winters, Erik Faulhaber, Jesse Chan, and Gregor Gassner. Adaptive numerical simulations with Trixi.jl: A case study of Julia for scientific computing. *Proceedings of the JuliaCon Conferences*, 1(1):77, 2022.
- [16] Andrés M Rueda-Ramírez, Benjamin Bolm, Dmitri Kuzmin, and Gregor J Gassner. Monolithic convex limiting for Legendre-Gauss-Lobatto discontinuous Galerkin spectral-element methods. *Communications on Applied Mathematics and Computation*, 6(3):1860–1898, 2024.
- [17] Michael Schlottke-Lakemper, Gregor J Gassner, Hendrik Ranocha, Andrew R Winters, Jesse Chan, and Andrés Rueda-Ramírez. Trixi.jl: Adaptive high-order numerical simulations of hyperbolic PDEs in Julia. <https://github.com/trixi-framework/Trixi.jl>, 2025.
- [18] Magnus Svärd. Entropy stable boundary conditions for the Euler equations. *Journal of Computational Physics*, 426:109947, 2021.
- [19] Magnus Svärd and Anita Gjesteland. Entropy-stable in-and outflow boundary conditions for the compressible Navier-Stokes equations. *arXiv preprint arXiv:2506.21065*, 2025.
- [20] François Vilar. Local subcell monolithic DG/FV convex property preserving scheme on unstructured grids and entropy consideration. *Journal of Computational Physics*, 521:113535, 2025.